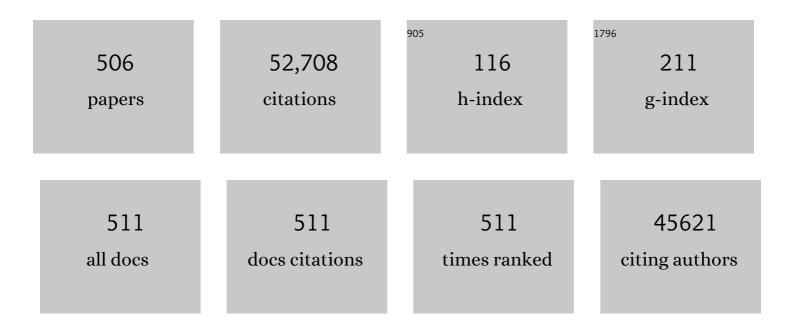
List of Publications by Year in descending order

Source: https://exaly.com/author-pdf/5049431/publications.pdf Version: 2024-02-01



#	Article	lF	CITATIONS
1	High rate and stable cycling of lithium metal anode. Nature Communications, 2015, 6, 6362.	5.8	1,954
2	Dendrite-Free Lithium Deposition via Self-Healing Electrostatic Shield Mechanism. Journal of the American Chemical Society, 2013, 135, 4450-4456.	6.6	1,736
3	Activation of surface lattice oxygen in single-atom Pt/CeO ₂ for low-temperature CO oxidation. Science, 2017, 358, 1419-1423.	6.0	1,114
4	Electrolyte additive enabled fast charging and stable cycling lithium metal batteries. Nature Energy, 2017, 2, .	19.8	1,048
5	Nitrogen-doped graphene and its electrochemical applications. Journal of Materials Chemistry, 2010, 20, 7491.	6.7	1,040
6	A Soft Approach to Encapsulate Sulfur: Polyaniline Nanotubes for Lithiumâ€ S ulfur Batteries with Long Cycle Life. Advanced Materials, 2012, 24, 1176-1181.	11.1	959
7	Oxidation of black carbon by biotic and abiotic processes. Organic Geochemistry, 2006, 37, 1477-1488.	0.9	942
8	Nitrogenâ€Coordinated Single Cobalt Atom Catalysts for Oxygen Reduction in Proton Exchange Membrane Fuel Cells. Advanced Materials, 2018, 30, 1706758.	11.1	788
9	Facile and controllable electrochemical reduction of graphene oxide and its applications. Journal of Materials Chemistry, 2010, 20, 743-748.	6.7	787
10	Stable cycling of high-voltage lithium metal batteries in ether electrolytes. Nature Energy, 2018, 3, 739-746.	19.8	767
11	Highâ€Voltage Lithiumâ€Metal Batteries Enabled by Localized Highâ€Concentration Electrolytes. Advanced Materials, 2018, 30, e1706102.	11.1	761
12	Natural oxidation of black carbon in soils: Changes in molecular form and surface charge along a climosequence. Geochimica Et Cosmochimica Acta, 2008, 72, 1598-1610.	1.6	733
13	Localized High-Concentration Sulfone Electrolytes for High-Efficiency Lithium-Metal Batteries. CheM, 2018, 4, 1877-1892.	5.8	628
14	Lewis Acid–Base Interactions between Polysulfides and Metal Organic Framework in Lithium Sulfur Batteries. Nano Letters, 2014, 14, 2345-2352.	4.5	623
15	Monolithic solid–electrolyte interphases formed in fluorinated orthoformate-based electrolytes minimize Li depletion and pulverization. Nature Energy, 2019, 4, 796-805.	19.8	621
16	Enhanced activity and stability of Pt catalysts on functionalized graphene sheets for electrocatalytic oxygen reduction. Electrochemistry Communications, 2009, 11, 954-957.	2.3	615
17	Enabling High-Voltage Lithium-Metal Batteries under Practical Conditions. Joule, 2019, 3, 1662-1676.	11.7	598
18	Monodispersed Coreâ^'Shell Fe3O4@Au Nanoparticles. Journal of Physical Chemistry B, 2005, 109, 21593-21601.	1.2	545

#	Article	IF	CITATIONS
19	Failure Mechanism for Fastâ€Charged Lithium Metal Batteries with Liquid Electrolytes. Advanced Energy Materials, 2015, 5, 1400993.	10.2	540
20	Performance enhancement and degradation mechanism identification of a single-atom Co–N–C catalyst for proton exchange membrane fuel cells. Nature Catalysis, 2020, 3, 1044-1054.	16.1	443
21	Controlling SEI Formation on SnSbâ€Porous Carbon Nanofibers for Improved Na Ion Storage. Advanced Materials, 2014, 26, 2901-2908.	11.1	441
22	Sensitive Immunosensor for Cancer Biomarker Based on Dual Signal Amplification Strategy of Graphene Sheets and Multienzyme Functionalized Carbon Nanospheres. Analytical Chemistry, 2010, 82, 2989-2995.	3.2	438
23	High-Efficiency Lithium Metal Batteries with Fire-Retardant Electrolytes. Joule, 2018, 2, 1548-1558.	11.7	436
24	Role of extracellular polymeric substances in bioflocculation of activated sludge microorganisms under glucose-controlled conditions. Water Research, 2010, 44, 4505-4516.	5.3	396
25	Redox properties of water on the oxidized and reduced surfaces of CeO2. Surface Science, 2003, 526, 1-18.	0.8	376
26	Extremely Stable Sodium Metal Batteries Enabled by Localized High-Concentration Electrolytes. ACS Energy Letters, 2018, 3, 315-321.	8.8	373
27	Hard carbon nanoparticles as high-capacity, high-stability anodic materials for Na-ion batteries. Nano Energy, 2016, 19, 279-288.	8.2	341
28	Bimetallic Cobaltâ€Based Phosphide Zeolitic Imidazolate Framework: CoP <i>_x</i> Phaseâ€Dependent Electrical Conductivity and Hydrogen Atom Adsorption Energy for Efficient Overall Water Splitting. Advanced Energy Materials, 2017, 7, 1601555.	10.2	340
29	Porous Silicon as a Versatile Platform for Laser Desorption/Ionization Mass Spectrometry. Analytical Chemistry, 2001, 73, 612-619.	3.2	337
30	Degradation Mechanisms of La–Sr–Co–Fe–O[sub 3] SOFC Cathodes. Electrochemical and Solid-State Letters, 2006, 9, A478.	2.2	329
31	Dendrite-Free Lithium Deposition with Self-Aligned Nanorod Structure. Nano Letters, 2014, 14, 6889-6896.	4.5	326
32	Non-encapsulation approach for high-performance Li–S batteries through controlled nucleation and growth. Nature Energy, 2017, 2, 813-820.	19.8	326
33	Thiophene hydrodesulfurization over nickel phosphide catalysts: effect of the precursor composition and support. Journal of Catalysis, 2005, 231, 300-313.	3.1	313
34	Nitrogen-doped mesoporous carbon for energy storage in vanadium redox flow batteries. Journal of Power Sources, 2010, 195, 4375-4379.	4.0	306
35	Functionalized Graphene Oxide as a Nanocarrier in a Multienzyme Labeling Amplification Strategy for Ultrasensitive Electrochemical Immunoassay of Phosphorylated p53 (S392). Analytical Chemistry, 2011, 83, 746-752.	3.2	305
36	Tuning Pt-CeO2 interactions by high-temperature vapor-phase synthesis for improved reducibility of lattice oxygen. Nature Communications, 2019, 10, 1358.	5.8	302

#	Article	IF	CITATIONS
37	High-Concentration Ether Electrolytes for Stable High-Voltage Lithium Metal Batteries. ACS Energy Letters, 2019, 4, 896-902.	8.8	302
38	Surface Plasmon-Driven Water Reduction: Gold Nanoparticle Size Matters. Journal of the American Chemical Society, 2014, 136, 9842-9845.	6.6	301
39	Joint Charge Storage for Highâ€Rate Aqueous Zinc–Manganese Dioxide Batteries. Advanced Materials, 2019, 31, e1900567.	11.1	299
40	High Voltage Operation of Niâ€Rich NMC Cathodes Enabled by Stable Electrode/Electrolyte Interphases. Advanced Energy Materials, 2018, 8, 1800297.	10.2	298
41	Dendrite-free Li deposition using trace-amounts of water as an electrolyte additive. Nano Energy, 2015, 15, 135-144.	8.2	297
42	Polyelectrolyte-Induced Reduction of Exfoliated Graphite Oxide: A Facile Route to Synthesis of Soluble Graphene Nanosheets. ACS Nano, 2011, 5, 1785-1791.	7.3	293
43	Manipulating surface reactions in lithium–sulphur batteries using hybrid anode structures. Nature Communications, 2014, 5, 3015.	5.8	290
44	Stability of biomass-derived black carbon in soils. Geochimica Et Cosmochimica Acta, 2008, 72, 6069-6078.	1.6	287
45	Hollow core–shell structured porous Si–C nanocomposites for Li-ion battery anodes. Journal of Materials Chemistry, 2012, 22, 11014.	6.7	280
46	Behavior of Lithium Metal Anodes under Various Capacity Utilization and High Current Density in Lithium Metal Batteries. Joule, 2018, 2, 110-124.	11.7	280
47	Toward Rational Design of Cu/SSZ-13 Selective Catalytic Reduction Catalysts: Implications from Atomic-Level Understanding of Hydrothermal Stability. ACS Catalysis, 2017, 7, 8214-8227. Instability, intermixing and electronic structure at the epitaxial <mml:math< td=""><td>5.5</td><td>278</td></mml:math<>	5.5	278
48	xmlns:mml="http://www.w3.org/1998/Math/MathML" altimg="si51.gif" display="inline" overflow="scroll"> <mml:msub><mml:mrow><mml:mstyle mathvariant="normal"><mml:mi>LaAlO</mml:mi></mml:mstyle </mml:mrow><mml:mrow><mml:mn>3<td>mn> <td>:mrow></td></td></mml:mn></mml:mrow></mml:msub>	mn> <td>:mrow></td>	:mrow>

#	Article	IF	CITATIONS
55	Supercritical fluid synthesis and characterization of catalytic metal nanoparticles on carbon nanotubes. Journal of Materials Chemistry, 2004, 14, 908.	6.7	246
56	Surface-Driven Sodium Ion Energy Storage in Nanocellular Carbon Foams. Nano Letters, 2013, 13, 3909-3914.	4.5	245
57	Highly Stable Operation of Lithium Metal Batteries Enabled by the Formation of a Transient Highâ€Concentration Electrolyte Layer. Advanced Energy Materials, 2016, 6, 1502151.	10.2	236
58	Ionic liquid-enhanced solid state electrolyte interface (SEI) for lithium–sulfur batteries. Journal of Materials Chemistry A, 2013, 1, 8464.	5.2	229
59	The adsorption of liquid and vapor water on TiO2(110) surfaces: the role of defects. Surface Science, 1995, 344, 237-250.	0.8	228
60	Surface characterization of nanomaterials and nanoparticles: Important needs and challenging opportunities. Journal of Vacuum Science and Technology A: Vacuum, Surfaces and Films, 2013, 31, 50820.	0.9	227
61	Self assembly of acetylcholinesterase on a gold nanoparticles–graphene nanosheet hybrid for organophosphate pesticide detection using polyelectrolyte as a linker. Journal of Materials Chemistry, 2011, 21, 5319.	6.7	219
62	Morphology and Electronic Structure of the Oxide Shell on the Surface of Iron Nanoparticles. Journal of the American Chemical Society, 2009, 131, 8824-8832.	6.6	218
63	Effect of nitrogen additives on flame retardant action of tributyl phosphate: Phosphorus–nitrogen synergism. Polymer Degradation and Stability, 2008, 93, 99-108.	2.7	213
64	Iron oxide–gold core–shell nanoparticles and thin film assembly. Journal of Materials Chemistry, 2005, 15, 1821.	6.7	211
65	Origin of lithium whisker formation and growth under stress. Nature Nanotechnology, 2019, 14, 1042-1047.	15.6	211
66	Nanoscale Alloying, Phase-Segregation, and Coreâ~'Shell Evolution of Goldâ^'Platinum Nanoparticles and Their Electrocatalytic Effect on Oxygen Reduction Reaction. Chemistry of Materials, 2010, 22, 4282-4294.	3.2	205
67	Development of high-temperature ferromagnetism inSnO2and paramagnetism in SnO by Fe doping. Physical Review B, 2005, 72, .	1.1	204
68	Effects of Electrolyte Salts on the Performance of Li–O ₂ Batteries. Journal of Physical Chemistry C, 2013, 117, 2635-2645.	1.5	204
69	The stability of organic solvents and carbon electrode in nonaqueous Li-O2 batteries. Journal of Power Sources, 2012, 215, 240-247.	4.0	197
70	Role of inner solvation sheath within salt–solvent complexes in tailoring electrode/electrolyte interphases for lithium metal batteries. Proceedings of the National Academy of Sciences of the United States of America, 2020, 117, 28603-28613.	3.3	191
71	Long-term black carbon dynamics in cultivated soil. Biogeochemistry, 2008, 89, 295-308.	1.7	186
72	Low-Temperature Pd/Zeolite Passive NO _{<i>x</i>} Adsorbers: Structure, Performance, and Adsorption Chemistry. Journal of Physical Chemistry C, 2017, 121, 15793-15803.	1.5	178

#	Article	IF	CITATIONS
73	XPS analysis of nanostructured materials and biological surfaces. Journal of Electron Spectroscopy and Related Phenomena, 2010, 178-179, 415-432.	0.8	177
74	Epitaxial growth and properties of cobalt-dopedZnOonαâ^'Al2O3single-crystal substrates. Physical Review B, 2004, 70, .	1.1	175
75	Highâ€Performance Silicon Anodes Enabled By Nonflammable Localized Highâ€Concentration Electrolytes. Advanced Energy Materials, 2019, 9, 1900784.	10.2	175
76	Ethanol synthesis from syngas over Rh-based/SiO2 catalysts: A combined experimental and theoretical modeling study. Journal of Catalysis, 2010, 271, 325-342.	3.1	174
77	Synergistic Catalysis between Pd and Fe in Gas Phase Hydrodeoxygenation of <i>m</i> -Cresol. ACS Catalysis, 2014, 4, 3335-3345.	5.5	173
78	Sensitive Immunoassay of a Biomarker Tumor Necrosis Factor-α Based on Poly(guanine)-Functionalized Silica Nanoparticle Label. Analytical Chemistry, 2006, 78, 6974-6979.	3.2	172
79	Selective Sorption of Cesium Using Self-Assembled Monolayers on Mesoporous Supports. Environmental Science & Technology, 2001, 35, 3962-3966.	4.6	168
80	Nanoscale effects on ion conductance of layer-by-layer structures of gadolinia-doped ceria and zirconia. Applied Physics Letters, 2005, 86, 131906.	1.5	168
81	Hidden ferromagnetic secondary phases in cobalt-doped ZnO epitaxial thin films. Physical Review B, 2008, 77, .	1.1	168
82	Reductive Sequestration of Pertechnetate (⁹⁹ TcO ₄ [–]) by Nano Zerovalent Iron (nZVI) Transformed by Abiotic Sulfide. Environmental Science & Technology, 2013, 47, 5302-5310.	4.6	162
83	Guided Lithium Metal Deposition and Improved Lithium Coulombic Efficiency through Synergistic Effects of LiAsF ₆ and Cyclic Carbonate Additives. ACS Energy Letters, 2018, 3, 14-19.	8.8	161
84	Effects of Reduction Temperature and Metalâ^'Support Interactions on the Catalytic Activity of Pt/γ-Al2O3 and Pt/TiO2 for the Oxidation of CO in the Presence and Absence of H2. Journal of Physical Chemistry B, 2005, 109, 23430-23443.	1.2	159
85	Advanced Electrolytes for Fastâ€Charging Highâ€Voltage Lithiumâ€Ion Batteries in Wideâ€Temperature Range. Advanced Energy Materials, 2020, 10, 2000368.	10.2	159
86	Coordination Chemistry in magnesium battery electrolytes: how ligands affect their performance. Scientific Reports, 2013, 3, 3130.	1.6	157
87	Tuning the Solid Electrolyte Interphase for Selective Li―and Naâ€ŀon Storage in Hard Carbon. Advanced Materials, 2017, 29, 1606860.	11.1	157
88	Ferromagnetism in chemically synthesized <mml:math xmlns:mml="http://www.w3.org/1998/Math/MathML" display="inline"><mml:mrow><mml:mi mathvariant="normal">Ce<mml:msub><mml:mi mathvariant="normal">O<mml:mn>2</mml:mn></mml:mi </mml:msub></mml:mi </mml:mrow>nanoparticle by Ni doping. Physical Review B, 2007, 76, .</mml:math 	1.1 25	156
89	Revisiting the Corrosion of the Aluminum Current Collector in Lithium-Ion Batteries. Journal of Physical Chemistry Letters, 2017, 8, 1072-1077.	2.1	156
90	Creation of variable concentrations of defects on TiO2(110) using low-density electron beams. Surface Science, 1994, 320, 295-306.	0.8	148

#	Article	IF	CITATIONS
91	Nitrogen–doped graphitized carbon shell encapsulated NiFe nanoparticles: A highly durable oxygen evolution catalyst. Nano Energy, 2017, 39, 245-252.	8.2	143
92	Addressing Passivation in Lithium–Sulfur Battery Under Lean Electrolyte Condition. Advanced Functional Materials, 2018, 28, 1707234.	7.8	143
93	The structure of Na2O–Al2O3–SiO2 glass: impact on sodium ion exchange in H2O and D2O. Journal of Non-Crystalline Solids, 2001, 296, 10-26.	1.5	142
94	Suppressing Lithium Dendrite Growth by Metallic Coating on a Separator. Advanced Functional Materials, 2017, 27, 1704391.	7.8	141
95	Comparative second harmonic generation and X-ray photoelectron spectroscopy studies of the UV creation and O2 healing of Ti3+ defects on (110) rutile TiO2 surfaces. Surface Science, 1995, 339, 114-124.	0.8	140
96	Infrared transparent spinel films with p-type conductivity. Thin Solid Films, 2001, 398-399, 45-52.	0.8	140
97	Highly Ordered Mesoporous Bimetallic Phosphides as Efficient Oxygen Evolution Electrocatalysts. ACS Energy Letters, 2016, 1, 792-796.	8.8	139
98	Characterization of CeO2-supported Cu–Pd bimetallic catalyst for the oxygen-assisted water–gas shift reaction. Journal of Catalysis, 2008, 260, 358-370.	3.1	138
99	Practical guides for x-ray photoelectron spectroscopy: First steps in planning, conducting, and reporting XPS measurements. Journal of Vacuum Science and Technology A: Vacuum, Surfaces and Films, 2019, 37, .	0.9	137
100	Low-solvation electrolytes for high-voltage sodium-ion batteries. Nature Energy, 2022, 7, 718-725.	19.8	137
101	Nucleophilic Displacements in Mixed Self-Assembled Monolayersâ€. Langmuir, 1996, 12, 5064-5075.	1.6	136
102	Correlation between Surface Chemistry, Density, and Band Gap in Nanocrystalline WO ₃ Thin Films. ACS Applied Materials & Interfaces, 2012, 4, 1371-1377.	4.0	135
103	Silicon (100)/SiO2 by XPS. Surface Science Spectra, 2013, 20, 36-42.	0.3	134
104	Long-term black carbon dynamics in cultivated soil. Biogeochemistry, 2009, 92, 163-176.	1.7	133
105	Minimal Proton Channel Enables H ₂ Oxidation and Production with a Water-Soluble Nickel-Based Catalyst. Journal of the American Chemical Society, 2013, 135, 18490-18496.	6.6	131
106	Effects of fluorinated solvents on electrolyte solvation structures and electrode/electrolyte interphases for lithium metal batteries. Proceedings of the National Academy of Sciences of the United States of America, 2021, 118, .	3.3	131
107	Enhanced performance of graphite anode materials by AIF3 coating for lithium-ion batteries. Journal of Materials Chemistry, 2012, 22, 12745.	6.7	129
108	Nanovoid Incorporated Ir _{<i>x</i>} Cu Metallic Aerogels for Oxygen Evolution Reaction Catalysis. ACS Energy Letters, 2018, 3, 2038-2044.	8.8	129

#	Article	IF	CITATIONS
109	Oneâ€Pot Process for Hydrodeoxygenation of Lignin to Alkanes Using Ruâ€Based Bimetallic and Bifunctional Catalysts Supported on Zeolite Y. ChemSusChem, 2017, 10, 1846-1856.	3.6	127
110	Reduction Mechanism of Fluoroethylene Carbonate for Stable Solid–Electrolyte Interphase Film on Silicon Anode. ChemSusChem, 2014, 7, 549-554.	3.6	126
111	Composition-Controlled Synthesis of Bimetallic Goldâ^'Silver Nanoparticles. Langmuir, 2004, 20, 11240-11246.	1.6	125
112	Dendriteâ€Free and Performanceâ€Enhanced Lithium Metal Batteries through Optimizing Solvent Compositions and Adding Combinational Additives. Advanced Energy Materials, 2018, 8, 1703022.	10.2	123
113	Designing Advanced In Situ Electrode/Electrolyte Interphases for Wide Temperature Operation of 4.5 V Li LiCoO ₂ Batteries. Advanced Materials, 2020, 32, e2004898.	11.1	123
114	Comparison of the sputter rates of oxide films relative to the sputter rate of SiO2. Journal of Vacuum Science and Technology A: Vacuum, Surfaces and Films, 2010, 28, 1060-1072.	0.9	122
115	Characterization challenges for nanomaterials. Surface and Interface Analysis, 2008, 40, 529-537.	0.8	121
116	Fluorescent dye encapsulated ZnO particles with cell-specific toxicity for potential use in biomedical applications. Journal of Materials Science: Materials in Medicine, 2009, 20, 11-22.	1.7	121
117	Correlation of Pt–Re surface properties with reaction pathways for the aqueous-phase reforming of glycerol. Journal of Catalysis, 2012, 287, 37-43.	3.1	118
118	Ultrafine and highly disordered Ni2Fe1 nanofoams enabled highly efficient oxygen evolution reaction in alkaline electrolyte. Nano Energy, 2018, 44, 319-326.	8.2	118
119	Highâ€Performance, Superparamagnetic, Nanoparticleâ€Based Heavy Metal Sorbents for Removal of Contaminants from Natural Waters. ChemSusChem, 2010, 3, 749-757.	3.6	117
120	Effects of Cesium Cations in Lithium Deposition via Self-Healing Electrostatic Shield Mechanism. Journal of Physical Chemistry C, 2014, 118, 4043-4049.	1.5	117
121	Effect of the Anion Activity on the Stability of Li Metal Anodes in Lithium‣ulfur Batteries. Advanced Functional Materials, 2016, 26, 3059-3066.	7.8	117
122	Porous Carbonâ€Hosted Atomically Dispersed Iron–Nitrogen Moiety as Enhanced Electrocatalysts for Oxygen Reduction Reaction in a Wide Range of pH. Small, 2018, 14, e1703118.	5.2	117
123	An advanced understanding of the specific effects of xylan and surface lignin contents on enzymatic hydrolysis of lignocellulosic biomass. Bioresource Technology, 2013, 132, 137-145.	4.8	115
124	Structure of the cleaved CaCO3(101̄4) surface in an aqueous environment. Surface Science, 1996, 351, 172-182.	0.8	114
125	XPS guide: Charge neutralization and binding energy referencing for insulating samples. Journal of Vacuum Science and Technology A: Vacuum, Surfaces and Films, 2020, 38, .	0.9	114
126	Spectroscopic Characterization of Extracellular Polymeric Substances from <i>Escherichia coli</i> and <i>Serratia marcescens</i> : Suppression Using Sub-Inhibitory Concentrations of Bismuth Thiols. Biomacromolecules, 2008, 9, 3079-3089.	2.6	113

#	Article	IF	CITATIONS
127	Nonflammable Electrolytes for Lithium Ion Batteries Enabled by Ultraconformal Passivation Interphases. ACS Energy Letters, 2019, 4, 2529-2534.	8.8	112
128	Structure Sensitivity of Acetylene Semi-Hydrogenation on Pt Single Atoms and Subnanometer Clusters. ACS Catalysis, 2019, 9, 11030-11041.	5.5	111
129	Effects of Imide–Orthoborate Dual-Salt Mixtures in Organic Carbonate Electrolytes on the Stability of Lithium Metal Batteries. ACS Applied Materials & Interfaces, 2018, 10, 2469-2479.	4.0	110
130	Adsorptive Removal of Organic Sulfur Compounds from Jet Fuel over K-Exchanged NiY Zeolites Prepared by Impregnation and Ion Exchange. Industrial & Engineering Chemistry Research, 2005, 44, 5740-5749.	1.8	106
131	Lithiumâ€Pretreated Hard Carbon as Highâ€Performance Sodiumâ€Ion Battery Anodes. Advanced Energy Materials, 2018, 8, 1801441.	10.2	105
132	Atomic-Structural Synergy for Catalytic CO Oxidation over Palladium–Nickel Nanoalloys. Journal of the American Chemical Society, 2014, 136, 7140-7151.	6.6	104
133	Complete Decomposition of Li ₂ CO ₃ in Li–O ₂ Batteries Using Ir/B ₄ C as Noncarbon-Based Oxygen Electrode. Nano Letters, 2017, 17, 1417-1424.	4.5	104
134	Chemical Processing in High-Pressure Aqueous Environments. 7. Process Development for Catalytic Gasification of Wet Biomass Feedstocks. Industrial & Engineering Chemistry Research, 2004, 43, 1999-2004.	1.8	103
135	The role of H2O in the carbonation of forsterite in supercritical CO2. International Journal of Greenhouse Gas Control, 2011, 5, 1081-1092.	2.3	103
136	Influence of Aging and Environment on Nanoparticle Chemistry: Implication to Confinement Effects in Nanoceria. Journal of Physical Chemistry C, 2012, 116, 14108-14114.	1.5	103
137	Electrocatalytic Hydrogen Evolution in Neutral pH Solutions: Dual-Phase Synergy. ACS Catalysis, 2019, 9, 8712-8718.	5.5	103
138	Surfaces with Reversible Hydrophilic/Hydrophobic Characteristics on Cross-linked Poly(N-isopropylacrylamide) Hydrogels. Langmuir, 2000, 16, 8016-8023.	1.6	102
139	Stability of polymer binders in Li–O 2 batteries. Journal of Power Sources, 2013, 243, 899-907.	4.0	102
140	Applications of XPS in the characterization of Battery materials. Journal of Electron Spectroscopy and Related Phenomena, 2019, 231, 2-10.	0.8	101
141	The corrosion of PEM fuel cell catalyst supports and its implications for developing durable catalysts. Electrochimica Acta, 2009, 54, 3109-3114.	2.6	100
142	Stabilization of Li Metal Anode in DMSOâ€Based Electrolytes via Optimization of Salt–Solvent Coordination for Li–O ₂ Batteries. Advanced Energy Materials, 2017, 7, 1602605.	10.2	99
143	Catalytic Roles of Co ⁰ and Co ²⁺ during Steam Reforming of Ethanol on Co/MgO Catalysts. ACS Catalysis, 2011, 1, 279-286.	5.5	98
144	Spatially Resolved Mineral Deposition on Patterned Self-Assembled Monolayers. Langmuir, 1994, 10, 619-622.	1.6	97

#	Article	IF	CITATIONS
145	Highly Reversible Sodium Ion Batteries Enabled by Stable Electrolyte-Electrode Interphases. ACS Energy Letters, 2020, 5, 3212-3220.	8.8	97
146	Correlation between Atomic Coordination Structure and Enhanced Electrocatalytic Activity for Trimetallic Alloy Catalysts. Journal of the American Chemical Society, 2011, 133, 12714-12727.	6.6	96
147	X-ray Photoelectron Spectroscopic Study of the Activation of Molecularly-Linked Gold Nanoparticle Catalysts. Langmuir, 2003, 19, 125-131.	1.6	93
148	Formation of Reversible Solid Electrolyte Interface on Graphite Surface from Concentrated Electrolytes. Nano Letters, 2017, 17, 1602-1609.	4.5	91
149	Interactions of HCOOH with stoichiometric and defective TiO2(110) surfaces. Surface Science, 1997, 380, 352-364.	0.8	90
150	Size Dependence of Lattice Parameter and Electronic Structure in CeO ₂ Nanoparticles. Inorganic Chemistry, 2020, 59, 5760-5767.	1.9	90
151	Advanced spectroscopic synchrotron techniques to unravel the intrinsic properties of dilute magnetic oxides: the case of Co:ZnO. New Journal of Physics, 2010, 12, 013020.	1.2	89
152	Role of Support–Nanoalloy Interactions in the Atomic-Scale Structural and Chemical Ordering for Tuning Catalytic Sites. Journal of the American Chemical Society, 2012, 134, 15048-15060.	6.6	89
153	Effect of Co/Ni ratios in cobalt nickel mixed oxide catalysts on methane combustion. Applied Catalysis A: General, 2015, 505, 62-69.	2.2	89
154	Simultaneous Stabilization of LiNi _{0.76} Mn _{0.14} Co _{0.10} O ₂ Cathode and Lithium Metal Anode by Lithium Bis(oxalato)borate as Additive. ChemSusChem, 2018, 11, 2211-2220.	3.6	89
155	Detrimental Effects of Chemical Crossover from the Lithium Anode to Cathode in Rechargeable Lithium Metal Batteries. ACS Energy Letters, 2018, 3, 2921-2930.	8.8	89
156	Effect of Co doping on the structural, optical and magnetic properties of ZnO nanoparticles. Journal of Physics Condensed Matter, 2007, 19, 266203.	0.7	88
157	Rational design of efficient electrode–electrolyte interfaces for solid-state energy storage using ion soft landing. Nature Communications, 2016, 7, 11399.	5.8	86
158	Gold–Copper Nanoparticles: Nanostructural Evolution and Bifunctional Catalytic Sites. Chemistry of Materials, 2012, 24, 4662-4674.	3.2	85
159	Mixed salts of LiTFSI and LiBOB for stable LiFePO4-based batteries at elevated temperatures. Journal of Materials Chemistry A, 2014, 2, 2346.	5.2	85
160	Tailoring the Local Environment of Platinum in Singleâ€Atom Pt ₁ /CeO ₂ Catalysts for Robust Lowâ€Temperature CO Oxidation. Angewandte Chemie - International Edition, 2021, 60, 26054-26062.	7.2	84
161	Interparticle Chiral Recognition of Enantiomers: A Nanoparticle-Based Regulation Strategy. Analytical Chemistry, 2009, 81, 689-698.	3.2	82
162	Reduction of U(VI) Incorporated in the Structure of Hematite. Environmental Science & Technology, 2012, 46, 9428-9436.	4.6	82

#	Article	IF	CITATIONS
163	Low-Temperature Synthesis of Tunable Mesoporous Crystalline Transition Metal Oxides and Applications as Au Catalyst Supports. Journal of Physical Chemistry C, 2008, 112, 13499-13509.	1.5	81
164	N incorporation and electronic structure in N-doped TiO2(110) rutile. Surface Science, 2007, 601, 1754-1762.	0.8	79
165	Intermetallic Pd ₃ Pb nanowire networks boost ethanol oxidation and oxygen reduction reactions with significantly improved methanol tolerance. Journal of Materials Chemistry A, 2017, 5, 23952-23959.	5.2	78
166	Water-induced formation of cobalt oxides over supported cobalt/ceria–zirconia catalysts under ethanol-steam conditions. Journal of Catalysis, 2010, 273, 229-235.	3.1	77
167	From Ultrafine Thiolate-Capped Copper Nanoclusters toward Copper Sulfide Nanodiscs: A Thermally Activated Evolution Route. Chemistry of Materials, 2010, 22, 261-271.	3.2	77
168	Electrochemically stable cathode current collectors for rechargeable magnesium batteries. Journal of Materials Chemistry A, 2014, 2, 2473-2477.	5.2	77
169	Suppressed oxygen extraction and degradation of LiNi x Mn y Co z O2 cathodes at high charge cut-off voltages. Nano Research, 2017, 10, 4221-4231.	5.8	77
170	Role of Inorganic Surface Layer on Solid Electrolyte Interphase Evolution at Li-Metal Anodes. ACS Applied Materials & Interfaces, 2019, 11, 31467-31476.	4.0	75
171	Controlled synthesis of highly-branched plasmonic gold nanoparticles through peptoid engineering. Nature Communications, 2018, 9, 2327.	5.8	74
172	Oxidative Remobilization of Technetium Sequestered by Sulfide-Transformed Nano Zerovalent Iron. Environmental Science & Technology, 2014, 48, 7409-7417.	4.6	73
173	Effects of structural defects on the electrochemical activation of Li2MnO3. Nano Energy, 2015, 16, 143-151.	8.2	73
174	Microbial and Mineralogical Characterizations of Soils Collected from the Deep Biosphere of the Former Homestake Gold Mine, South Dakota. Microbial Ecology, 2010, 60, 539-550.	1.4	70
175	Advanced Lowâ€Flammable Electrolytes for Stable Operation of Highâ€Voltage Lithiumâ€Ion Batteries. Angewandte Chemie - International Edition, 2021, 60, 12999-13006.	7.2	70
176	PdCuPt Nanocrystals with Multibranches for Enzyme-Free Glucose Detection. ACS Applied Materials & Interfaces, 2016, 8, 22196-22200.	4.0	68
177	Reduction and Simultaneous Removal of ⁹⁹ Tc and Cr by Fe(OH) ₂ (s) Mineral Transformation. Environmental Science & Technology, 2017, 51, 8635-8642.	4.6	68
178	Defining Active Catalyst Structure and Reaction Pathways from ab Initio Molecular Dynamics and Operando XAFS: Dehydrogenation of Dimethylaminoborane by Rhodium Clusters. Journal of the American Chemical Society, 2009, 131, 10516-10524.	6.6	67
179	New insights into reaction mechanisms of ethanol steam reforming on Co–ZrO2. Applied Catalysis B: Environmental, 2015, 162, 141-148.	10.8	67
180	Stabilization of Super Electrophilic Pd ⁺² Cations in Small-Pore SSZ-13 Zeolite. Journal of Physical Chemistry C, 2020, 124, 309-321.	1.5	67

#	Article	IF	CITATIONS
181	Low Pt-content ternary PdCuPt nanodendrites: an efficient electrocatalyst for oxygen reduction reaction. Nanoscale, 2017, 9, 1279-1284.	2.8	66
182	Assigning Oxidation States to Organic Compounds via Predictions from X-ray Photoelectron Spectroscopy: A Discussion of Approaches and Recommended Improvements. Journal of Chemical Education, 2014, 91, 232-238.	1.1	65
183	Molecular Storage of Mg Ions with Vanadium Oxide Nanoclusters. Advanced Functional Materials, 2016, 26, 3446-3453.	7.8	65
184	B4C as a stable non-carbon-based oxygen electrode material for lithium-oxygen batteries. Nano Energy, 2017, 33, 195-204.	8.2	65
185	Sugar Blowingâ€Induced Porous Cobalt Phosphide/Nitrogenâ€Doped Carbon Nanostructures with Enhanced Electrochemical Oxidation Performance toward Water and Other Small Molecules. Small, 2017, 13, 1700796.	5.2	65
186	Polymerâ€inâ€â€œQuasiâ€ionic Liquid―Electrolytes for Highâ€Voltage Lithium Metal Batteries. Advanced Ener Materials, 2019, 9, 1902108.	gy _{10.2}	65
187	Optimization of fluorinated orthoformate based electrolytes for practical high-voltage lithium metal batteries. Energy Storage Materials, 2021, 34, 76-84.	9.5	65
188	The ion beam materials analysis laboratory at the environmental molecular sciences laboratory. Nuclear Instruments and Methods in Physics Research, Section A: Accelerators, Spectrometers, Detectors and Associated Equipment, 1999, 420, 81-89.	0.7	64
189	Magnetic gas sensing using a dilute magnetic semiconductor. Applied Physics Letters, 2006, 89, 112509.	1.5	64
190	Heterogeneous reduction of U6+ by structural Fe2+ from theory and experiment. Geochimica Et Cosmochimica Acta, 2011, 75, 7277-7290.	1.6	64
191	Controlling Surface Phase Transition and Chemical Reactivity of O3-Layered Metal Oxide Cathodes for High-Performance Na-Ion Batteries. ACS Energy Letters, 2020, 5, 1718-1725.	8.8	64
192	Use and limitations of electron flood gun control of surface potential during XPS: two non-homogeneous sample types. Surface and Interface Analysis, 2002, 33, 781-790.	0.8	63
193	In2O3/Al2O3 Catalysts for NOx Reduction in Lean Condition. Journal of Catalysis, 2002, 210, 97-105.	3.1	63
194	Comparative Study on the Sulfur Tolerance and Carbon Resistance of Supported Noble Metal Catalysts in Steam Reforming of Liquid Hydrocarbon Fuel. ACS Catalysis, 2012, 2, 1127-1137.	5.5	63
195	Three-dimensional PtNi hollow nanochains as an enhanced electrocatalyst for the oxygen reduction reaction. Journal of Materials Chemistry A, 2016, 4, 8755-8761.	5.2	63
196	Role of Metal Coordination Structures in Enhancement of Electrocatalytic Activity of Ternary Nanoalloys for Oxygen Reduction Reaction. ACS Catalysis, 2012, 2, 795-806.	5.5	62
197	The Mechanisms of Oxygen Reduction and Evolution Reactions in Nonaqueous Lithium–Oxygen Batteries. ChemSusChem, 2014, 7, 2436-2440.	3.6	62
198	An Advanced Na–FeCl ₂ ZEBRA Battery for Stationary Energy Storage Application. Advanced Energy Materials, 2015, 5, 1500357.	10.2	62

#	Article	IF	CITATIONS
199	Introductory guide to backgrounds in XPS spectra and their impact on determining peak intensities. Journal of Vacuum Science and Technology A: Vacuum, Surfaces and Films, 2020, 38, .	0.9	62
200	Inhibition of Trace Element Release During Fe(II)-Activated Recrystallization of Al-, Cr-, and Sn-Substituted Goethite and Hematite. Environmental Science & Technology, 2012, 46, 10031-10039.	4.6	61
201	First step towards the growth of single-crystal oxides on Si: Formation of a two-dimensional crystalline silicate on Si(001). Applied Physics Letters, 2001, 79, 3591-3593.	1.5	60
202	Very Stable Electron Field Emission from Strontium Titanate Coated Carbon Nanotube Matrices with Low Emission Thresholds. ACS Nano, 2013, 7, 117-125.	7.3	60
203	Surface Plasmon Mediated Chemical Solution Deposition of Gold Nanoparticles on a Nanostructured Silver Surface at Room Temperature. Journal of the American Chemical Society, 2013, 135, 38-41.	6.6	60
204	A Facile Method for Synthesizing Dendritic Core–Shell Structured Ternary Metallic Aerogels and Their Enhanced Electrochemical Performances. Chemistry of Materials, 2016, 28, 7928-7934.	3.2	60
205	Excellent Cycling Stability of Sodium Anode Enabled by a Stable Solid Electrolyte Interphase Formed in Etherâ€Based Electrolytes. Advanced Functional Materials, 2020, 30, 2001151.	7.8	60
206	Morphology and oxide shell structure of iron nanoparticles grown by sputter-gas-aggregation. Nanotechnology, 2007, 18, 255603.	1.3	59
207	Molecular structures of polymer/sulfur composites for lithium–sulfur batteries with long cycle life. Journal of Materials Chemistry A, 2013, 1, 9517.	5.2	59
208	Dendrimerâ€Encapsulated Ruthenium Oxide Nanoparticles as Catalysts in Lithiumâ€Oxygen Batteries. Advanced Functional Materials, 2014, 24, 7510-7519.	7.8	59
209	Electrodeposition from Acidic Solutions of Nickel Bis(benzenedithiolate) Produces a Hydrogen-Evolving Ni–S Film on Glassy Carbon. ACS Catalysis, 2014, 4, 90-98.	5.5	59
210	Proliferation of Faulty Materials Data Analysis in the Literature. Microscopy and Microanalysis, 2020, 26, 1-2.	0.2	59
211	Enhanced Stability of Lithium Metal Anode by using a 3D Porous Nickel Substrate. ChemElectroChem, 2018, 5, 761-769.	1.7	58
212	Rational Design of Electrolytes for Long-Term Cycling of Si Anodes over a Wide Temperature Range. ACS Energy Letters, 2021, 6, 387-394.	8.8	58
213	MOCVD growth and structure of Nb- and V-doped TiO2 films on sapphire. Journal of Crystal Growth, 2000, 212, 178-190.	0.7	57
214	Oxidation of H2S by Iron Oxides in Unsaturated Conditions. Environmental Science & Technology, 2003, 37, 2192-2199.	4.6	55
215	Redoxâ€Active Metal–Organic Composites for Highly Selective Oxygen Separation Applications. Advanced Materials, 2016, 28, 3572-3577.	11.1	55
216	Quantifying the Impact of Nanoparticle Coatings and Nonuniformities on XPS Analysis: Gold/Silver Core–Shell Nanoparticles. Analytical Chemistry, 2016, 88, 3917-3925.	3.2	55

#	Article	IF	CITATIONS
217	Beam damage of selfâ€assembled monolayers. Journal of Vacuum Science and Technology A: Vacuum, Surfaces and Films, 1993, 11, 2292-2297.	0.9	54
218	Chemical sensors based on dielectric response of functionalized mesoporous silica films. Journal of Materials Research, 2001, 16, 2810-2816.	1.2	54
219	Graphene oxide membranes with high permeability and selectivity for dehumidification of air. Carbon, 2016, 106, 164-170.	5.4	54
220	Ultrathin dendritic IrTe nanotubes for an efficient oxygen evolution reaction in a wide pH range. Journal of Materials Chemistry A, 2018, 6, 8855-8859.	5.2	54
221	Ultrafine Pd ensembles anchored-Au2Cu aerogels boost ethanol electrooxidation. Nano Energy, 2018, 53, 206-212.	8.2	54
222	Electron beam-induced thickening of the protective oxide layer around Fe nanoparticles. Ultramicroscopy, 2007, 108, 43-51.	0.8	53
223	A General Mechanism for Stabilizing the Small Sizes of Precious Metal Nanoparticles on Oxide Supports. Chemistry of Materials, 2014, 26, 5475-5481.	3.2	53
224	Kinetically Controlled Synthesis of Pt-Based One-Dimensional Hierarchically Porous Nanostructures with Large Mesopores as Highly Efficient ORR Catalysts. ACS Applied Materials & Interfaces, 2016, 8, 35213-35218.	4.0	53
225	Electrolyte Regulating toward Stabilization of Cobalt-Free Ultrahigh-Nickel Layered Oxide Cathode in Lithium-Ion Batteries. ACS Energy Letters, 2021, 6, 1324-1332.	8.8	53
226	Stabilizing ultrahigh-nickel layered oxide cathodes for high-voltage lithium metal batteries. Materials Today, 2021, 44, 15-24.	8.3	53
227	Multiâ€instrument characterization of the surfaces and materials in microfabricated, carbon nanotubeâ€ŧemplated thin layer chromatography plates. An analogy to †The Blind Men and the Elephant'. Surface and Interface Analysis, 2013, 45, 1273-1282.	0.8	52
228	Nitrogen and Fluorineâ€Codoped Carbon Nanowire Aerogels as Metalâ€Free Electrocatalysts for Oxygen Reduction Reaction. Chemistry - A European Journal, 2017, 23, 10460-10464.	1.7	52
229	An Ionâ€Imprinting Derived Strategy to Synthesize Singleâ€Atom Iron Electrocatalysts for Oxygen Reduction. Small, 2021, 17, e2004454.	5.2	52
230	Molecular-confinement of polysulfides within mesoscale electrodes for the practical application of lithium sulfur batteries. Nano Energy, 2015, 13, 267-274.	8.2	50
231	Room-temperature ferromagnetism in ion-implanted Co-doped TiO2(110) rutile. Applied Physics Letters, 2004, 84, 4466-4468.	1.5	49
232	ZnO nanoclusters: Synthesis and photoluminescence. Applied Physics Letters, 2005, 87, 241917.	1.5	49
233	A Hydrogen-Evolving Ni(P ₂ N ₂) ₂ Electrocatalyst Covalently Attached to a Glassy Carbon Electrode: Preparation, Characterization, and Catalysis. Comparisons with the Homogeneous Analogue. Inorganic Chemistry, 2014, 53, 6875-6885.	1.9	49
234	Core–shell PdPb@Pd aerogels with multiply-twinned intermetallic nanostructures: facile synthesis with accelerated gelation kinetics and their enhanced electrocatalytic properties. Journal of Materials Chemistry A, 2018, 6, 7517-7521.	5.2	49

#	Article	IF	CITATIONS
235	Dynamic Lattice Oxygen Participation on Perovskite LaNiO ₃ during Oxygen Evolution Reaction. Journal of Physical Chemistry C, 2020, 124, 15386-15390.	1.5	49
236	Adsorption and Reaction of CO and CO2on Oxidized and Reduced SrTiO3(100) Surfaces. Journal of Physical Chemistry B, 2005, 109, 10327-10331.	1.2	48
237	Adsorption of Amelogenin onto Self-Assembled and Fluoroapatite Surfaces. Journal of Physical Chemistry B, 2009, 113, 1833-1842.	1.2	48
238	XAS and XPS Characterization of Monolayers Derived from a Dithiol and Structurally Related Disulfide-Containing Polyamides. Langmuir, 2002, 18, 8123-8128.	1.6	47
239	Surface and Interface Control on Photochemically Initiated Immobilization. Journal of the American Chemical Society, 2006, 128, 14067-14072.	6.6	47
240	Chromium-assisted synthesis of platinum nanocube electrocatalysts. Chemical Communications, 2010, 46, 7184.	2.2	46
241	Interfacial chemistry and the performance of bromine-etched CdZnTe radiation detector devices. IEEE Transactions on Nuclear Science, 2002, 49, 2005-2009.	1.2	45
242	Functionalized TiO2Nanoparticles for Use for in Situ Anion Immobilization. Environmental Science & Technology, 2005, 39, 7306-7310.	4.6	45
243	Coreâ^'Shell-Structured Magnetic Ternary Nanocubes. Journal of the American Chemical Society, 2010, 132, 17686-17689.	6.6	45
244	A Facile Solvothermal Synthesis of Octahedral Fe ₃ O ₄ Nanoparticles. Small, 2015, 11, 2649-2653.	5.2	45
245	U(<scp>v</scp>) in metal uranates: a combined experimental and theoretical study of MgUO ₄ , CrUO ₄ , and FeUO ₄ . Dalton Transactions, 2016, 45, 4622-4632.	1.6	45
246	Two-Dimensional N,S-Codoped Carbon/Co ₉ S ₈ Catalysts Derived from Co(OH) ₂ Nanosheets for Oxygen Reduction Reaction. ACS Applied Materials & Interfaces, 2017, 9, 36755-36761.	4.0	45
247	A comparative study of pomegranate Sb@C yolk–shell microspheres as Li and Na-ion battery anodes. Nanoscale, 2019, 11, 348-355.	2.8	45
248	Optimized Electrolyte with High Electrochemical Stability and Oxygen Solubility for Lithium–Oxygen and Lithium–Air Batteries. ACS Energy Letters, 2020, 5, 2182-2190.	8.8	45
249	Noncovalent Functionalization of Carbon Nanotubes with Molecular Anchors Using Supercritical Fluidsâ€. Journal of Physical Chemistry B, 2004, 108, 8737-8741.	1.2	44
250	Synthesis of lutetium phosphate–apoferritin core–shell nanoparticles for potential applications in radioimmunoimaging and radioimmunotherapy of cancers. Journal of Materials Chemistry, 2008, 18, 1779.	6.7	44
251	Thiolâ^ Ene Induced Diphosphonic Acid Functionalization of Superparamagnetic Iron Oxide Nanoparticles. Langmuir, 2010, 26, 12285-12292.	1.6	44
252	Effects of cell positive cans and separators on the performance of high-voltage Li-ion batteries. Journal of Power Sources, 2012, 213, 160-168.	4.0	44

#	Article	IF	CITATIONS
253	Formation of Interfacial Layer and Long-Term Cyclability of Li–O ₂ Batteries. ACS Applied Materials & Interfaces, 2014, 6, 14141-14151.	4.0	44
254	Highly uniform distribution of Pt nanoparticles on N-doped hollow carbon spheres with enhanced durability for oxygen reduction reaction. RSC Advances, 2017, 7, 6303-6308.	1.7	44
255	Kinetically controlled synthesis of AuPt bi-metallic aerogels and their enhanced electrocatalytic performances. Journal of Materials Chemistry A, 2017, 5, 19626-19631.	5.2	44
256	Conversion of Methane into Methanol and Ethanol over Nickel Oxide on Ceria–Zirconia Catalysts in a Single Reactor. Angewandte Chemie - International Edition, 2017, 56, 13876-13881.	7.2	44
257	Decorating β′′-alumina solid-state electrolytes with micron Pb spherical particles for improving Na wettability at lower temperatures. Journal of Materials Chemistry A, 2018, 6, 19703-19711.	5.2	44
258	Constructing Robust Electrode/Electrolyte Interphases to Enable Wide Temperature Applications of Lithium-Ion Batteries. ACS Applied Materials & Interfaces, 2019, 11, 21496-21505.	4.0	44
259	Reversible Electrochemical Interface of Mg Metal and Conventional Electrolyte Enabled by Intermediate Adsorption. ACS Energy Letters, 2020, 5, 200-206.	8.8	44
260	X-ray Photoelectron Spectroscopy Studies of Oxidized and Reduced CeO2(111) Surfaces. Surface Science Spectra, 2004, 11, 73-81.	0.3	43
261	Nonstoichiometric material transfer in the pulsed laser deposition of LaAlO3. Applied Physics Letters, 2010, 97, .	1.5	43
262	Effects of Propylene Carbonate Content in CsPF ₆ -Containing Electrolytes on the Enhanced Performances of Graphite Electrode for Lithium-Ion Batteries. ACS Applied Materials & Interfaces, 2016, 8, 5715-5722.	4.0	43
263	Structural identification of ZnxZryOz catalysts for Cascade aldolization and self-deoxygenation reactions. Applied Catalysis B: Environmental, 2018, 234, 337-346.	10.8	43
264	Self-organizing layers from complex molecular anions. Nature Communications, 2018, 9, 1889.	5.8	43
265	Enabling Natural Graphite in Highâ€Voltage Aqueous Graphite Zn Metal Dualâ€Ion Batteries. Advanced Energy Materials, 2020, 10, 2001256.	10.2	43
266	Gold–polyaniline composites : Part II. Effects of nanometer sized particles. Physical Chemistry Chemical Physics, 2005, 7, 3619.	1.3	42
267	Epitaxial growth and microstructure of Cu2O nanoparticle/thin films on SrTiO3(100). Nanotechnology, 2007, 18, 115601.	1.3	42
268	Suppression of conductivity in Mn-doped ZnO thin films. Journal of Applied Physics, 2009, 105, .	1.1	42
269	Stable, microfabricated thin layer chromatography plates without volume distortion on patterned, carbon and Al2O3-primed carbon nanotube forests. Journal of Chromatography A, 2012, 1257, 195-203.	1.8	42
270	Cr(III) Adsorption by Cluster Formation on Boehmite Nanoplates in Highly Alkaline Solution. Environmental Science & Technology, 2019, 53, 11043-11055.	4.6	42

#	Article	IF	CITATIONS
271	Changes in the quaternary structure of amelogenin when adsorbed onto surfaces. Biopolymers, 2009, 91, 103-107.	1.2	41
272	The Role of Cesium Cation in Controlling Interphasial Chemistry on Graphite Anode in Propylene Carbonate-Rich Electrolytes. ACS Applied Materials & Interfaces, 2015, 7, 20687-20695.	4.0	41
273	Structure and thermodynamics of uranium-containing iron garnets. Geochimica Et Cosmochimica Acta, 2016, 189, 269-281.	1.6	41
274	The importance of solid electrolyte interphase formation for long cycle stability full-cell Na-ion batteries. Nano Energy, 2016, 27, 664-672.	8.2	41
275	Reaction of soda lime silicate glass in isotopically labelled water. Journal of Non-Crystalline Solids, 1986, 86, 369-380.	1.5	40
276	Evidence for Localization of Reaction upon Reduction of Carbon Tetrachloride by Granular Iron. Langmuir, 2002, 18, 7688-7693.	1.6	39
277	Immersion Deposition of Metal Films on Silicon and Germanium Substrates in Supercritical Carbon Dioxide. Chemistry of Materials, 2003, 15, 83-91.	3.2	39
278	Growth, microstructure and electrical properties of sputter-deposited hafnium oxide (HfO2) thin films grown using a HfO2 ceramic target. Applied Surface Science, 2011, 257, 2197-2202.	3.1	39
279	The Role of Iron-Bearing Minerals in NO ₂ to HONO Conversion on Soil Surfaces. Environmental Science & Technology, 2016, 50, 8649-8660.	4.6	39
280	Effects of Fluorinated Diluents in Localized High oncentration Electrolytes for Lithium–Oxygen Batteries. Advanced Functional Materials, 2021, 31, 2002927.	7.8	39
281	N incorporation, composition and electronic structure in N-doped TiO2(001) anatase epitaxial films grown on LaAlO3(001). Surface Science, 2008, 602, 133-141.	0.8	38
282	Revealing the Dynamics of Platinum Nanoparticle Catalysts on Carbon in Oxygen and Water Using Environmental TEM. ACS Catalysis, 2017, 7, 7658-7664.	5.5	38
283	Enhanced Cyclability of Lithium–Oxygen Batteries with Electrodes Protected by Surface Films Induced via In Situ Electrochemical Process. Advanced Energy Materials, 2018, 8, 1702340.	10.2	38
284	Electrochemical investigation of polyhalide ion oxidation–reduction on carbon nanotube electrodes for redox flow batteries. Electrochemistry Communications, 2009, 11, 2064-2067.	2.3	36
285	The Effect of Zinc Addition on the Oxidation State of Cobalt in Co/ZrO ₂ Catalysts. ChemSusChem, 2011, 4, 1679-1684.	3.6	36
286	Electrocatalytic properties of poly(3,4-ethylenedioxythiophene) (PEDOT) in Li-O2 battery. Electrochemistry Communications, 2013, 29, 63-66.	2.3	36
287	A perspective on two chemometrics tools: PCA and MCR, and introduction of a new one: Pattern recognition entropy (PRE), as applied to XPS and ToF-SIMS depth profiles of organic and inorganic materials. Applied Surface Science, 2018, 433, 994-1017.	3.1	36
288	Interactions of liquid and vapor water with stoichiometric and defective TiO2(100) surfaces. Surface Science, 1999, 440, 60-68.	0.8	35

#	Article	IF	CITATIONS
289	Reaction of hydroquinone with hematite. Journal of Colloid and Interface Science, 2004, 274, 433-441.	5.0	35
290	Enabling Ether-Based Electrolytes for Long Cycle Life of Lithium-Ion Batteries at High Charge Voltage. ACS Applied Materials & Interfaces, 2020, 12, 54893-54903.	4.0	35
291	Introduction to topical collection: Reproducibility challenges and solutions with a focus on guides to XPS analysis. Journal of Vacuum Science and Technology A: Vacuum, Surfaces and Films, 2021, 39, .	0.9	35
292	Inâ€Situâ€Grown ZnCo ₂ O ₄ on Singleâ€Walled Carbon Nanotubes as Air Electrode Materials for Rechargeable Lithium–Oxygen Batteries. ChemSusChem, 2015, 8, 3697-3703.	3.6	34
293	Template-directed synthesis of nitrogen- and sulfur-codoped carbon nanowire aerogels with enhanced electrocatalytic performance for oxygen reduction. Nano Research, 2017, 10, 1888-1895.	5.8	34
294	Block copolymer templated synthesis of PtIr bimetallic nanocatalysts for the formic acid oxidation reaction. Journal of Materials Chemistry A, 2017, 5, 21514-21527.	5.2	34
295	Freestanding NiFe Oxyfluoride Holey Film with Ultrahigh Volumetric Capacitance for Flexible Asymmetric Supercapacitors. Small, 2018, 14, 1702295.	5.2	34
296	Single-Step Conversion of Ethanol to <i>n</i> Butene over Ag-ZrO ₂ /SiO ₂ Catalysts. ACS Catalysis, 2020, 10, 10602-10613.	5.5	34
297	An investigation of hydrogen depth profiling using ToFâ€SIMS. Surface and Interface Analysis, 2012, 44, 232-237.	0.8	33
298	Versailles Project on Advanced Materials and Standards Interlaboratory Study on Measuring the Thickness and Chemistry of Nanoparticle Coatings Using XPS and LEIS. Journal of Physical Chemistry C, 2016, 120, 24070-24079.	1.5	33
299	Direct determination of volume changes in ion-beam-irradiated SiC. Journal of Applied Physics, 2004, 95, 4687-4690.	1.1	32
300	Probing cation antisite disorder inGd2Ti2O7pyrochlore by site-specific near-edge x-ray-absorption fine structure and x-ray photoelectron spectroscopy. Physical Review B, 2004, 70, .	1.1	32
301	Spectroscopic Characterizations of Molecularly Linked Gold Nanoparticle Assemblies upon Thermal Treatment. Langmuir, 2004, 20, 4254-4260.	1.6	32
302	Soft landing of bare PtRu nanoparticles for electrochemical reduction of oxygen. Nanoscale, 2015, 7, 12379-12391.	2.8	32
303	Third Row Transition Metals by X-ray Photoelectron Spectroscopy. Surface Science Spectra, 2000, 7, 1-68.	0.3	31
304	Development and processing temperature dependence of ferromagnetism in Zn0.98Co0.02O. Journal of Applied Physics, 2006, 99, 08M123.	1.1	31
305	Mitigation of Sulfur Poisoning of Ni/Zirconia SOFC Anodes by Antimony and Tin. Journal of the Electrochemical Society, 2011, 158, B424.	1.3	31
306	Stability of polymeric separators in lithium metal batteries in a low voltage environment. Journal of Materials Chemistry A, 2018, 6, 5006-5015.	5.2	31

#	Article	IF	CITATIONS
307	Comparative SHG and XPS studies of interactions between defects and N2O on rutile TiO2(110) surfaces. Surface Science, 1997, 392, 1-7.	0.8	30
308	Novel magnetic hydrogen sensing: a case study using antiferromagnetic haematite nanoparticles. Nanotechnology, 2007, 18, 165502.	1.3	30
309	On the Relationship between Nonstoichiometry and Passivity Breakdown in Ultrathin Oxides: Combined Depth-Dependent Spectroscopy, Mottâ^Schottky Analysis, and Molecular Dynamics Simulation Studies. Journal of Physical Chemistry C, 2009, 113, 3502-3511.	1.5	30
310	Stabilization of ZnMnO3 phase from sol–gel synthesized nitrate precursors. Journal of Sol-Gel Science and Technology, 2010, 53, 141-147.	1.1	30
311	Temperature Dependence of the Oxygen Reduction Mechanism in Nonaqueous Li–O ₂ Batteries. ACS Energy Letters, 2017, 2, 2525-2530.	8.8	30
312	Edge Dislocations Induce Improved Photocatalytic Efficiency of Colored TiO ₂ . Advanced Materials Interfaces, 2019, 6, 1901121.	1.9	30
313	Chemical bonding and electronic structures of the Al2SiO5 polymorphs, andalusite, sillimanite, and kyanite: X-ray photoelectron- and electron energy loss spectroscopy studies. American Mineralogist, 2006, 91, 740-746.	0.9	29
314	The synthesis of Ag-doped mesoporous TiO2. Microporous and Mesoporous Materials, 2008, 111, 639-642.	2.2	29
315	Performance of solid oxide fuel cells operated with coal syngas provided directly from a gasification process. Journal of Power Sources, 2012, 214, 142-152.	4.0	29
316	Al2O3 e-Beam Evaporated onto Silicon (100)/SiO2, by XPS. Surface Science Spectra, 2013, 20, 43-48.	0.3	29
317	The role of FeS in initial activation and performance degradation of Na–NiCl2 batteries. Journal of Power Sources, 2014, 272, 398-403.	4.0	29
318	Charge-Coupled Substituted Garnets (Y _{3–<i>x</i>} Ca _{0.5<i>x</i>} M _{0.5<i>x</i>})Fe ₅ O _{12(M = Ce, Th): Structure and Stability as Crystalline Nuclear Waste Forms. Inorganic Chemistry, 2015, 54, 4156-4166.}	ub> 1.9	29
319	Fractal character of crack propagation in epoxy and epoxy composites as revealed by photon emission during fracture. Journal of Materials Research, 1991, 6, 183-195.	1.2	28
320	Three-dimensional Nitrogen-Doped Reduced Graphene Oxide/Carbon Nanotube Composite Catalysts for Vanadium Flow Batteries. Electroanalysis, 2017, 29, 1469-1473.	1.5	28
321	Optimization of Magnesiumâ€Doped Lithium Metal Anode for High Performance Lithium Metal Batteries through Modeling and Experiment. Angewandte Chemie - International Edition, 2021, 60, 16506-16513.	7.2	28
322	A Polymer-in-Salt Electrolyte with Enhanced Oxidative Stability for Lithium Metal Polymer Batteries. ACS Applied Materials & Interfaces, 2021, 13, 31583-31593.	4.0	28
323	Electrochemistry of TiN in 6 M KOH Solution. Journal of the Electrochemical Society, 1998, 145, 1211-1218.	1.3	27
324	Adsorption and Reaction of Methanol on Stoichiometric and Defective SrTiO3(100) Surfaces. Journal of Physical Chemistry B, 2005, 109, 4507-4513.	1.2	27

#	Article	IF	CITATIONS
325	Effects of tungsten oxide addition on the electrochemical performance of nanoscale tantalum oxide-based electrocatalysts for proton exchange membrane (PEM) fuel cells. Journal of Power Sources, 2011, 196, 6099-6103.	4.0	27
326	Bifunctional nanoparticles for SERS monitoring and magnetic intervention of assembly and enzyme cutting of DNAs. Journal of Materials Chemistry B, 2013, 1, 4320.	2.9	27
327	Comparison of 20 nm silver nanoparticles synthesized with and without a gold core: Structure, dissolution in cell culture media, and biological impact on macrophages. Biointerphases, 2015, 10, 031003.	0.6	27
328	Ambient temperature NO oxidation over Cr-based amorphous mixed oxide catalysts: effects from the second oxide components. Catalysis Science and Technology, 2017, 7, 2362-2370.	2.1	27
329	Behavior of Si and C atoms in ion amorphized SiC. Journal of Applied Physics, 2007, 101, 023524.	1.1	26
330	Controlling size of gold clusters in polyaniline from top–down and from bottom–up. Journal of Electroanalytical Chemistry, 2008, 621, 238-244.	1.9	26
331	Influence of samaria doping on the resistance of ceria thin films and its implications to the planar oxygen sensing devices. Sensors and Actuators B: Chemical, 2009, 139, 380-386.	4.0	26
332	Electrically Switched Ion Exchange Based on Carbon-Polypyrrole Composite Smart Materials for the Removal of ReO ₄ [–] from Aqueous Solutions. Environmental Science & Technology, 2019, 53, 2612-2617.	4.6	26
333	Holeâ€Trappingâ€Induced Stabilization of Ni ^{4 +} in SrNiO ₃ /LaFeO ₃ Superlattices. Advanced Materials, 2020, 32, e2005003.	11.1	26
334	X-ray photoelectron spectroscopic analyses of corrosion products formed on rock bolt carbon steel in chloride media with bicarbonate and silicate ions. Corrosion Science, 2004, 46, 2629-2649.	3.0	25
335	Irradiation behavior of SrTiO[sub 3] at temperatures close to the critical temperature for amorphization. Journal of Applied Physics, 2006, 100, 113533.	1.1	25
336	<mml:math <br="" xmlns:mml="http://www.w3.org/1998/Math/MathML">display="inline"><mml:mrow><mml:msub><mml:mrow><mml:mi>UO</mml:mi></mml:mrow><mml:mn>2Corrosion by Nonclassical Diffusion. Physical Review Letters, 2015, 114, 246103.</mml:mn></mml:msub></mml:mrow></mml:math>	ז ו:nan פא <td>າml2ສsub></td>	າml 2ສ sub>
337	A lithium-sulfur battery with a solution-mediated pathway operating under lean electrolyte conditions. Nano Energy, 2020, 76, 105041.	8.2	25
338	Inorganic tin aluminophosphate nanocomposite for reductive separation of pertechnetate. Environmental Science: Nano, 2016, 3, 1003-1013.	2.2	24
339	Controlling Ion Coordination Structure and Diffusion Kinetics for Optimized Electrode-Electrolyte Interphases and High-Performance Si Anodes. Chemistry of Materials, 2020, 32, 8956-8964.	3.2	24
340	Toward the Practical Use of Cobalt-Free Lithium-Ion Batteries by an Advanced Ether-Based Electrolyte. ACS Applied Materials & Interfaces, 2021, 13, 44339-44347.	4.0	24
341	Effect of Mn doping on the structural, morphological, optical and magnetic properties of indium tin oxide films. Journal of Materials Science: Materials in Electronics, 2007, 18, 1197-1201.	1.1	23
342	Unravelling high-temperature stability of lithium-ion battery with lithium-rich oxide cathode in localized high-concentration electrolyte. Journal of Power Sources Advances, 2020, 5, 100024.	2.6	23

#	Article	IF	CITATIONS
343	Approach for determining area selectivity in small-area XPS analysis. Surface and Interface Analysis, 2000, 29, 766-772.	0.8	22
344	Role of dopant incorporation on the magnetic properties of Ce1â^'xNixO2 nanoparticles: An electron paramagnetic resonance study. Journal of Applied Physics, 2008, 103, .	1.1	22
345	Electrochemically Controlled Atom by Atom Deposition of Gold to Polyaniline. Journal of the Electrochemical Society, 2010, 157, P83.	1.3	22
346	Investigation of Copper(I) Oxide Quantum Dots by Near-Edge X-ray Absorption Fine Structure Spectroscopy. Chemistry of Materials, 2003, 15, 3939-3946.	3.2	21
347	Electrophilic Aromatic Substitutions of Amine and Sulfonate onto Fine-Grained Activated Carbon for Aqueous-Phase Metal Ion Removal. Separation Science and Technology, 2004, 39, 3263-3279.	1.3	21
348	Ferromagnetism in Ti-Doped ZnO Nanoclusters Above Room Temperature. IEEE Transactions on Magnetics, 2006, 42, 2697-2699.	1.2	21
349	Growth and structure of epitaxial Ce0.8Sm0.2O1.9 by oxygen-plasma-assisted molecular beam epitaxy. Journal of Crystal Growth, 2008, 310, 2450-2456.	0.7	21
350	Microstructure of the Native Oxide Layer on Ni and Cr-Doped Ni Nanoparticles. Journal of Nanoscience and Nanotechnology, 2011, 11, 8488-8497.	0.9	21
351	Incorporation of Np(V) and U(VI) in carbonate and sulfate minerals crystallized from aqueous solution. Geochimica Et Cosmochimica Acta, 2015, 151, 133-149.	1.6	21
352	Conversion of ethanol to 1,3–butadiene over Ag–ZrO2/SiO2 catalysts: The role of surface interfaces. Journal of Energy Chemistry, 2021, 54, 7-15.	7.1	21
353	Sulfone-based electrolytes for high energy density lithium-ion batteries. Journal of Power Sources, 2022, 527, 231171.	4.0	21
354	Ferromagnetic semiconductor nanoclusters: Co-doped Cu2O. Applied Physics Letters, 2007, 90, 013106.	1.5	20
355	As-Received,Ozone Cleaned and Ar+ Sputtered Surfaces of Hafnium Oxide Grown by Atomic Layer Deposition and Studied by XPS. Surface Science Spectra, 2011, 18, 46-57.	0.3	20
356	Characterization of natural titanomagnetites (Fe3â^'xTixO4) for studying heterogeneous electron transfer to Tc(VII) in the Hanford subsurface. Geochimica Et Cosmochimica Acta, 2014, 128, 114-127.	1.6	20
357	Dopant distribution, oxygen stoichiometry and magnetism of nanoscale Sn0.99Co0.01O2. Solid State Communications, 2006, 139, 434-438.	0.9	19
358	On the room-temperature ferromagnetism of Zn1â^'xCrxO thin films deposited by reactive co-sputtering. Solar Energy Materials and Solar Cells, 2007, 91, 1496-1502.	3.0	19
359	The synthesis of cadmium doped mesoporous TiO2. Inorganic Chemistry Communication, 2007, 10, 639-641.	1.8	19
360	Multiwalled Carbon Nanotube Forest Grown via Chemical Vapor Deposition from Iron Catalyst Nanoparticles, by XPS. Surface Science Spectra, 2013, 20, 62-67.	0.3	19

#	Article	IF	CITATIONS
361	Investigating commercial cellulase performances toward specific biomass recalcitrance factors using reference substrates. Applied Microbiology and Biotechnology, 2014, 98, 4409-4420.	1.7	19
362	Probing the Origin of Interfacial Carriers in SrTiO ₃ –LaCrO ₃ Superlattices. Chemistry of Materials, 2017, 29, 1147-1155.	3.2	19
363	Synthesis of nanometer-sized fayalite and magnesium-iron(II) mixture olivines. Journal of Colloid and Interface Science, 2018, 515, 129-138.	5.0	19
364	Steam reforming of simulated bio-oil on K-Ni-Cu-Mg-Ce-O/Al2O3: The effect of K. Catalysis Today, 2019, 323, 183-190.	2.2	19
365	Surface engineering of earth-abundant Fe catalysts for selective hydrodeoxygenation of phenolics in liquid phase. Chemical Science, 2020, 11, 5874-5880.	3.7	19
366	High performance sodium-sulfur batteries at low temperature enabled by superior molten Na wettability. Chemical Communications, 2021, 57, 45-48.	2.2	19
367	Preparation, Characterization and Anion Exchange Properties of Polypyrrole/Carbon Nanotube Nanocomposites. Journal of Nanoscience and Nanotechnology, 2006, 6, 547-553.	0.9	18
368	Ultrafine Particulate Ferrous Iron and Anthracene Associations with Mitochondrial Dysfunction. Aerosol Science and Technology, 2011, 45, 1109-1122.	1.5	18
369	Nitrogen-incorporation induced changes in the microstructure of nanocrystalline WO3 thin films. Thin Solid Films, 2011, 520, 1446-1450. Heterogeneous growth of cadmium and cobalt carbonate phases at the <mml:math< td=""><td>0.8</td><td>18</td></mml:math<>	0.8	18
370	xmlns:mml="http://www.w3.org/1998/Math/MathML" altimg="si1.gif" overflow="scroll"> <mml:mfenced open="(" close=")"><mml:mrow><mml:mn>10</mml:mn><mml:mover accent="true"><mml:mn>1</mml:mn><mml:mo stretchy="true">Â⁻<mml:mn>4</mml:mn></mml:mo </mml:mover </mml:mrow></mml:mfenced 	1.4	18
371	calcite surface. Chemical Geology, 2015, 397, 24-36. A Highâ€Performance Na–Al Battery Based on Reversible NaAlCl ₄ Catholyte. Advanced Energy Materials, 2020, 10, 2001378.	10.2	18
372	Surface decontamination of simulated chemical warfare agents using a nonequilibrium plasma with off-gas monitoring. IEEE Transactions on Plasma Science, 2002, 30, 1454-1459.	0.6	17
373	Synthesis of room-temperature ferromagnetic Cr-doped TiO2(1 1 0) rutile single crystals using ion implantation. Nuclear Instruments & Methods in Physics Research B, 2006, 242, 198-200.	0.6	17
374	Effects of Sulfation Level on the Desulfation Behavior of Presulfated Pt-BaO/Al ₂ O ₃ Lean NO <i>_x</i> Trap Catalysts: A Combined H ₂ Temperature-Programmed Reaction, in Situ Sulfur K-Edge X-ray Absorption Near-Edge Spectroscopy, X-ray Photoelectron Spectroscopy, and Time-Resolved X-ray Diffraction Study. Journal	1.5	17
375	of Physical Chemistry C, 2009, 113, 7336-7341. Watermelon-like iron nanoparticles: Cr doping effect on magnetism and magnetization interaction reversal. Nanoscale, 2013, 5, 7872.	2.8	17
376	Continuous precipitation of ceria nanoparticles from a continuous flow micromixer. International Journal of Advanced Manufacturing Technology, 2013, 64, 579-586.	1.5	17
377	Adsorption and Reaction of Acetaldehyde on Stoichiometric and Defective SrTiO3(100) Surfaces. Journal of Physical Chemistry B, 2004, 108, 1646-1652.	1.2	16
378	Sweeping potential regulated structural and chemical evolution of solid-electrolyte interphase on Cu and Li as revealed by cryo-TEM. Nano Energy, 2020, 76, 105040.	8.2	16

#	Article	IF	CITATIONS
379	Advanced Lowâ€Flammable Electrolytes for Stable Operation of Highâ€Voltage Lithiumâ€lon Batteries. Angewandte Chemie, 2021, 133, 13109-13116.	1.6	16
380	Distribution of oxygen vacancies and gadolinium dopants in ZrO2–CeO2 multi-layer films grown on α-Al2O3. Solid State Ionics, 2006, 177, 1299-1306.	1.3	15
381	Growth and characterization of highly oriented gadolinia-doped ceria (111) thin films on zirconia (111)/sapphire (0001) substrates. Thin Solid Films, 2008, 516, 6088-6094.	0.8	15
382	Superior nanoscale passive oxide layers synthesized under photon irradiation for environmental protection. Applied Physics Letters, 2008, 92, 263103.	1.5	15
383	Growth and Characterization of Barium Oxide Nanoclusters on YSZ(111). Journal of Physical Chemistry C, 2009, 113, 14324-14328 Chemistry C, 2009, 113, 14324-14328 Epitaxial Feemmi:math xmlns:mml="http://www.w3.org/1998/Math/MathML"	1.5	15
384	display="inline"> <mml:msub><mml:mrow /><mml:mrow><mml:mn>3</mml:mn><mml:mo>â^'</mml:mo><mml:mi>x</mml:mi></mml:mrow></mml:mrow </mml:msub> xmlns:mml="http://www.w3.org/1998/Math/MathML" display="inline"> <mml:mi>x</mml:mi> /> <mml:mi>x</mml:mi> O <mml:math< td=""><td>1.1</td><td>th>Ti<mml:r 15</mml:r </td></mml:math<>	1.1	th>Ti <mml:r 15</mml:r
385	xmlns:mml="http://www.w3.org/1998/Math/MathML" display="inline"> <mml:msub><mml:mrow /><mml: X-Ray Photoelectron Spectroscopy Applications. , 2017, , 716-724.</mml: </mml:mrow </mml:msub>		15
386	Correlative surface imaging reveals chemical signatures for bacterial hotspots on plant roots. Analyst, The, 2020, 145, 393-401.	1.7	15
387	Sequential Ammonia and Carbon Dioxide Adsorption on Pyrolyzed Biomass to Recover Waste Stream Nutrients. ACS Sustainable Chemistry and Engineering, 2020, 8, 7121-7131.	3.2	15
388	Surface electronic properties and site-specific laser desorption processes of highly structured nanoporous MgO thin films. Surface Science, 2005, 593, 242-247.	0.8	14
389	Metalorganic chemical vapor deposition of carbon-free ZnO using the bis(2,2,6,6-tetramethyl-3,5-heptanedionato)zinc precursor. Journal of Materials Research, 2007, 22, 1230-1234.	1.2	14
390	Growth-rate induced epitaxial orientation of CeO2 on Al2O3(0001). Applied Physics Letters, 2009, 94, 204101.	1.5	14
391	Transition metal dopants essential for producing ferromagnetism in metal oxide nanoparticles. Physical Review B, 2010, 82, .	1.1	14
392	Thickness Dependency of Thin-Film Samaria-Doped Ceria for Oxygen Sensing. IEEE Sensors Journal, 2011, 11, 217-224.	2.4	14
393	Thermally Evaporated Iron (Oxide) on an Alumina Barrier Layer, by XPS. Surface Science Spectra, 2013, 20, 49-54.	0.3	14
394	Covalent attachment of diphosphine ligands to glassy carbon electrodes via Cu-catalyzed alkyne-azide cycloaddition. Metallation with Ni(<scp>ii</scp>). Dalton Transactions, 2015, 44, 12225-12233.	1.6	14
395	Electrical and Magnetic Properties Modification in Heavy Ion Irradiated Nanograin Ni _{<i>x</i>} Co _(3–<i>x</i>) O ₄ Films. Journal of Physical Chemistry C, 2015, 119, 22465-22476.	1.5	14
396	Fabrication of electrocatalytic Ta nanoparticles by reactive sputtering and ion soft landing. Journal of Chemical Physics, 2016, 145, 174701.	1.2	14

#	Article	IF	CITATIONS
397	Electrochemically Controlled Ionâ€exchange Property of Carbon Nanotubes/Polypyrrole Nanocomposite in Various Electrolyte Solutions. Electroanalysis, 2017, 29, 929-936.	1.5	14
398	Calcareous organic matter coatings sequester siderophores in alkaline soils. Science of the Total Environment, 2020, 724, 138250.	3.9	14
399	Conductivity of Oriented Samaria-Doped Ceria Thin Films Grown by Oxygen-Plasma-Assisted Molecular Beam Epitaxy. Electrochemical and Solid-State Letters, 2008, 11, B76.	2.2	13
400	Compositional tuning of ultrathin surface oxides on metal and alloy substrates using photons: Dynamic simulations and experiments. Physical Review B, 2010, 81, .	1.1	13
401	Syntrophic Effects in a Subsurface Clostridial Consortium on Fe(III)-(Oxyhydr)oxide Reduction and Secondary Mineralization. Geomicrobiology Journal, 2014, 31, 101-115.	1.0	13
402	Vacuum Cleaved Calcium Carbonate by XPS. Surface Science Spectra, 1999, 6, 153-159.	0.3	12
403	Supercritical fluid immersion deposition: a new process for selective deposition of metal films on silicon substrates. Surface and Coatings Technology, 2005, 190, 25-31.	2.2	12
404	Synthesis and characterization of phosphate-coated mesoporous titania and Cd-doping of same via ion-exchange. Inorganic Chemistry Communication, 2007, 10, 642-645.	1.8	12
405	Incorporation of Cu acceptors in ZnO nanocrystals. Journal of Applied Physics, 2010, 108, 064301.	1.1	12
406	The effect of ion irradiation on the dissolution of UO2 and UO2-based simulant fuel. Journal of Alloys and Compounds, 2018, 735, 1350-1356.	2.8	12
407	High energy ion beam studies of ion exchange in a Na2O–Al2O3–SiO2 glass. Journal of Applied Physics, 2002, 91, 1910-1920.	1.1	11
408	Temperature-induced phase separation in chromium films. Applied Physics Letters, 2003, 82, 2230-2232.	1.5	11
409	Erosion rate variations during XPS sputter depth profiling of nanoporous films. Surface and Interface Analysis, 2005, 37, 417-423.	0.8	11
410	Effects of atmospheres on bonding characteristics of silver and alumina. International Journal of Hydrogen Energy, 2008, 33, 4001-4011.	3.8	11
411	Photochemical Reactions of Poly(4â€vinylphenol) Thin Films. Macromolecular Chemistry and Physics, 2010, 211, 461-470.	1.1	11
412	Effect of sulfur loading on the desulfation chemistry of a commercial lean NOx trap catalyst. Catalysis Today, 2012, 197, 3-8.	2.2	11
413	Thermally Annealed Iron (Oxide) Thin Film on an Alumina Barrier Layer, by XPS. Surface Science Spectra, 2013, 20, 55-61.	0.3	11
414	Impact of a Mixed Oxide's Surface Composition and Structure on Its Adsorptive Properties: Case of the (Fe,Cr) ₃ O ₄ (111) Termination of the α-(Fe,Cr) ₂ O ₃ (0001) Surface. Journal of Physical Chemistry C, 2014, 118, 29058-29067.	1.5	11

#	Article	IF	CITATIONS
415	Cr(VI) Effect on Tc-99 Removal from Hanford Low-Activity Waste Simulant by Ferrous Hydroxide. Environmental Science & Technology, 2018, 52, 11752-11759.	4.6	11
416	Electronic response of aluminum-bearing minerals. Journal of Chemical Physics, 2018, 149, 024502.	1.2	11
417	Understanding the Deactivation of Agâ^'ZrO ₂ /SiO ₂ Catalysts for the Singleâ€step Conversion of Ethanol to Butenes. ChemCatChem, 2021, 13, 999-1008.	1.8	11
418	Polyacrylonitrile Composites of Ag–Al–Si–O Aerogels and Xerogels as Iodine and Iodide Sorbents. ACS Applied Polymer Materials, 2021, 3, 3344-3353.	2.0	11
419	Interaction of HCOOH with stoichiometric and reduced SrTiO3(100) surfaces. Journal of Vacuum Science and Technology A: Vacuum, Surfaces and Films, 2000, 18, 1893-1899.	0.9	10
420	The Electrode as Organolithium Reagent: Catalyst-Free Covalent Attachment of Electrochemically Active Species to an Azide-Terminated Glassy Carbon Electrode Surface. Inorganic Chemistry, 2013, 52, 13674-13684.	1.9	10
421	Spectroscopic Characterization of Aqua [<i>fac</i> -Tc(CO) ₃] ⁺ Complexes at High Ionic Strength. Inorganic Chemistry, 2018, 57, 6903-6912.	1.9	10
422	In situ molecular imaging of adsorbed protein films in water indicating hydrophobicity and hydrophilicity. Scientific Reports, 2020, 10, 3695.	1.6	10
423	Practical Aspects of Charging Phenomena in XPS as Demonstrated in Oxidized-Al Films on Al and Al Alloys. Journal of Surface Analysis (Online), 2002, 9, 396-403.	0.1	9
424	Electronic structure of ytterbium-doped strontium fluoroapatite: Photoemission and photoabsorption investigation. Journal of Applied Physics, 2002, 91, 5135-5140.	1.1	8
425	Physical properties and surface/interface analysis of nanocrystalline WO3 films grown under variable oxygen gas flow rates. Applied Surface Science, 2012, 259, 172-177.	3.1	8
426	Effect of Cr(III) Adsorption on the Dissolution of Boehmite Nanoparticles in Caustic Solution. Environmental Science & Technology, 2020, 54, 6375-6384.	4.6	8
427	Elucidating the Active Site and the Role of Alkali Metals in Selective Hydrodeoxygenation of Phenols over Ironâ€Carbideâ€based Catalyst. ChemSusChem, 2021, 14, 4546-4555.	3.6	8
428	Selective Removal of Perfluorobutyric Acid Using an Electroactive Ion Exchanger Based on Polypyrrole@Iron Oxide on Carbon Cloth. ACS Applied Materials & Interfaces, 2021, 13, 48500-48507.	4.0	8
429	Facile Dual-Protection Layer and Advanced Electrolyte Enhancing Performances of Cobalt-free/Nickel-rich Cathodes in Lithium-Ion Batteries. ACS Applied Materials & Interfaces, 2022, 14, 17405-17414.	4.0	8
430	Interfacial Engineering with a Nanoparticle-Decorated Porous Carbon Structure on β″-Alumina Solid-State Electrolytes for Molten Sodium Batteries. ACS Applied Materials & Interfaces, 2022, 14, 25534-25544.	4.0	8
431	Hydrogen bubbles and formation of nanoporous silicon during electrochemical etching. Surface and Interface Analysis, 2005, 37, 555-561.	0.8	7
432	Effect of Coal Gas Contaminants on Solid Oxide Fuel Cell Operation. ECS Transactions, 2008, 11, 63-70.	0.3	7

#	Article	IF	CITATIONS
433	Functional mesoporous carbon built from the 1,10-phenanthroline building block: A new class of catalyst support. Inorganic Chemistry Communication, 2007, 10, 1541-1544.	1.8	7
434	Study of surface cleaning methods and pyrolysis temperatures on nanostructured carbon films using x-ray photoelectron spectroscopy. Journal of Vacuum Science and Technology A: Vacuum, Surfaces and Films, 2012, 30, 061407.	0.9	7
435	Microstructure and Cs Behavior of Ba-Doped Aluminosilicate Pollucite Irradiated with F ⁺ Ions. Journal of Physical Chemistry C, 2014, 118, 18160-18169.	1.5	7
436	Tailoring the Local Environment of Platinum in Singleâ€Atom Pt ₁ /CeO ₂ Catalysts for Robust Lowâ€Temperature CO Oxidation. Angewandte Chemie, 2021, 133, 26258-26266.	1.6	7
437	Aluminum Nitride-Silicon Carbide Alloy Crystals Grown on SiC Substrates by Sublimation. MRS Internet Journal of Nitride Semiconductor Research, 2005, 10, 1.	1.0	6
438	Nucleation and Growth of MOCVD Grown (Cr, Zn)O Films. Journal of the Electrochemical Society, 2007, 154, D134.	1.3	6
439	Magnetic interaction reversal in watermelon nanostructured Cr-doped Fe nanoclusters. Applied Physics Letters, 2013, 103, .	1.5	6
440	Growth and surface modification of LaFeO3 thin films induced by reductive annealing. Applied Surface Science, 2015, 330, 309-315.	3.1	6
441	Gold/silver core-shell 20 nm nanoparticles extracted from citrate solution examined by XPS. Surface Science Spectra, 2016, 23, 29-39.	0.3	6
442	Multimodal and <i>In-Situ</i> Chemical Imaging of Critical Surfaces and Interfaces in Li Batteries. Microscopy Today, 2016, 24, 32-39.	0.2	6
443	Structure and thermodynamic stability of UTa ₃ O ₁₀ , a U(<scp>v</scp>)-bearing compound. Dalton Transactions, 2016, 45, 18892-18899.	1.6	6
444	Highly Stable Oxygen Electrodes Enabled by Catalyst Redistribution through an In Situ Electrochemical Method. Advanced Energy Materials, 2019, 9, 1803598.	10.2	6
445	Bimetallic Ir _{<i>x</i>} Pb nanowire networks with enhanced electrocatalytic activity for the oxygen evolution reaction. Journal of Materials Chemistry A, 2022, 10, 11196-11204.	5.2	6
446	Influence of adsorbed and implanted sulfur on the corrosion of iron in calcium nitrate at 60 °C. Journal of Vacuum Science and Technology A: Vacuum, Surfaces and Films, 1992, 10, 3007-3011.	0.9	5
447	Beam Damage of Poly(2-chloroethyl methylacrylate) [PCEMA] Films as Observed by X-ray Photoelectron Spectroscopy at 143 K, 303 K, and 373 K. Surface Science Spectra, 2003, 10, 80-100.	0.3	5
448	Simple method for estimating and comparing x-ray damage rates. Journal of Vacuum Science and Technology A: Vacuum, Surfaces and Films, 2005, 23, 1740-1744.	0.9	5
449	Direct measurement of oxygen incorporation into thin film oxides at room temperature upon ultraviolet photon irradiation. Applied Physics Letters, 2008, 93, .	1.5	5
450	Raman and XPS characterization of fuel–cladding interactions using miniature specimens. Journal of Nuclear Materials, 2009, 383, 237-243.	1.3	5

#	Article	IF	CITATIONS
451	Analysis of Fe nanoparticles using XPS measurements under d.c. or pulsedâ€voltage bias. Surface and Interface Analysis, 2010, 42, 859-862.	0.8	5
452	Surface speciation and interactions between adsorbed chloride and water on cerium dioxide. Journal of Solid State Chemistry, 2018, 262, 16-25.	1.4	5
453	Molecular Iodine Interactions with Fe, Ni, Cr, and Stainless Steel Alloys. Industrial & Engineering Chemistry Research, 2021, 60, 2447-2454.	1.8	5
454	Optimization of Magnesiumâ€Doped Lithium Metal Anode for High Performance Lithium Metal Batteries through Modeling and Experiment. Angewandte Chemie, 2021, 133, 16642-16649.	1.6	5
455	Atomic Force Microscopy and Infrared Nanospectroscopy of COVID-19 Spike Protein for the Quantification of Adhesion to Common Surfaces. Langmuir, 2021, 37, 12089-12097.	1.6	5
456	Effects of high-temperature CeO ₂ calcination on the activity of Pt/CeO ₂ catalysts for oxidation of unburned hydrocarbon fuels. Catalysis Science and Technology, 2022, 12, 2462-2470.	2.1	5
457	A freeze-thaw molten salt battery for seasonal storage. Cell Reports Physical Science, 2022, 3, 100821.	2.8	5
458	Enhancing Moisture Stability of Sulfide Solid-State Electrolytes by Reversible Amphipathic Molecular Coating. ACS Applied Materials & Interfaces, 2022, 14, 32035-32042.	4.0	5
459	The Microstructure, Phase and Ferroelectric Properties of PZT Thin Films on Oriented Multilayer Electrodes. Materials Research Society Symposia Proceedings, 1999, 596, 199.	0.1	4
460	Performance of bare and sol-gel-coated DKDP crystal surfaces exposed to multiple 351-nm laser pulses in vacuum and air. , 2002, , .		4
461	Correlation among Channeling, Morphological, and Microstructural Properties in Epitaxial CeO[sub 2] Films. Electrochemical and Solid-State Letters, 2006, 9, J17.	2.2	4
462	Electrodeposition of technetium on platinum for thermal ionization mass spectrometry (TIMS). Journal of Radioanalytical and Nuclear Chemistry, 2008, 276, 493-498.	0.7	4
463	Fine Structural Features and Electronic Structure of Core-Shell Structured Fe Nanoparticles Probed using TEM/STEM and EELS. Microscopy and Microanalysis, 2009, 15, 1204-1205.	0.2	4
464	Gallium arsenide (GaAs) (001) after sublimation of arsenic (As) thin-film cap, by XPS. Surface Science Spectra, 2016, 23, 83-92.	0.3	4
465	The Effect of Solvent on the Capacity Retention in a Germanium Anode for Lithium Ion Batteries. Journal of Electrochemical Energy Conversion and Storage, 2018, 15, .	1.1	4
466	Lithiumâ€Metal Batteries: Highâ€Voltage Lithiumâ€Metal Batteries Enabled by Localized Highâ€Concentration Electrolytes (Adv. Mater. 21/2018). Advanced Materials, 2018, 30, 1870144.	11.1	4
467	Preparation of nanoparticles for surface analysis. , 2020, , 295-347.		4
468	X-ray photoelectron spectroscopy data from lightly Pd doped TiO2 anatase nanoparticles. Surface Science Spectra, 2020, 27, .	0.3	4

#	Article	IF	CITATIONS
469	Plasma etching of lead germanate (PGO) ferroelectric thin film. Journal of Vacuum Science and Technology A: Vacuum, Surfaces and Films, 2001, 19, 1341-1345.	0.9	3
470	Microstructure and secondary phase segregation correlation in epitaxial/oriented ZnO films with unfavorable Cr dopant. Journal of Materials Research, 2009, 24, 506-515.	1.2	3
471	Promotional Effect of CO2 on Desulfation Processes for Pre-Sulfated Pt-BaO/Al2O3 Lean NOx Trap Catalysts. Topics in Catalysis, 2009, 52, 1719-1722.	1.3	3
472	Tetragonal-Like Phase in Core–Shell Iron Iron-Oxide Nanoclusters. Journal of Physical Chemistry C, 2017, 121, 11794-11803.	1.5	3
473	The Influence of Transitional Metal Dopants on Reducing Chlorine Evolution during the Electrolysis of Raw Seawater. Applied Sciences (Switzerland), 2021, 11, 11911.	1.3	3
474	The Adsorption of Liquid and Vapor Water on TiO ₂ (110) Surfaces: The Role of Defects. Materials Research Society Symposia Proceedings, 1994, 357, 97.	0.1	2
475	Analyzing localized corrosion in lon-implanted metals via XPS/AES. Jom, 2001, 53, 37-41.	0.9	2
476	Characterizations of Core-Shell Nanoparticle Catalysts for Methanol Electrooxidation. Materials Research Society Symposia Proceedings, 2002, 756, 1.	0.1	2
477	Characterization of Microstructure and Composition of Fe-B Nanobars as Biosensor Platform. Materials Research Society Symposia Proceedings, 2006, 962, 1.	0.1	2
478	Electrochemical effects of S accumulation on ion-implanted Alloy 22 in 1M NaCl solutions. Corrosion Science, 2007, 49, 2497-2511.	3.0	2
479	Accelerated testing of HT-9 with zirconia coatings containing gallium using Raman Spectroscopy and XPS. Journal of Nuclear Materials, 2009, 395, 23-29.	1.3	2
480	Using Thin Films to Screen Possible Scintillator Materials. IEEE Transactions on Nuclear Science, 2009, 56, 1650-1654.	1.2	2
481	An Electrochemically Activated Nanofilm for Sustainable Mg Anode with Fast Charge Transfer Kinetics. Journal of the Electrochemical Society, 2021, 168, 120519.	1.3	2
482	Biomimetic Lithography and Deposition Kinetics of Iron Oxyhydroxide Thin Films. Materials Research Society Symposia Proceedings, 1993, 330, 139.	0.1	1
483	The Interaction of Liquid and Vapor Water with Nearly Defect-Free and Defective TiO2(100) Surfaces. Materials Research Society Symposia Proceedings, 1996, 432, 45.	0.1	1
484	Corrosion of Phosphorusâ€Implanted 304L Stainless Steel in 1 N  H 2 SO 4. Journal of the Elec Society, 1999, 146, 984-987.	trochemic 1.3	cal 1
485	X-ray Photoelectron Spectroscopy Studies of Oxidized and Reduced Ce0.8Zr0.2O2(111) Surfaces. Surface Science Spectra, 2004, 11, 82-90.	0.3	1
486	Synthesis and characterization of compositionally graded Si1â^'xGex layers on Si substrate. Nuclear Instruments & Methods in Physics Research B, 2007, 261, 723-726.	0.6	1

#	Article	IF	CITATIONS
487	Fabrication of SiO2 microdisk arrays for optics and light trapping experiments. Microelectronic Engineering, 2007, 84, 2799-2803.	1.1	1
488	Variation of Oxygen-to-Carbon Ratio in Oxyacetylene Flame. , 2008, , .		1
489	Performance Evaluation of an Oxygen Sensor as a Function of the Samaria Doped Ceria Film Thickness. Materials Research Society Symposia Proceedings, 2009, 1209, 1.	0.1	1
490	The Importance of Complementary Information Provided by Surface Analysis, Electron Microscopy and in situ Characterization of Nanoparticles. Microscopy and Microanalysis, 2010, 16, 408-409.	0.2	1
491	Mechanistic Studies on Room Temperature Photoexcitation Effects on Passivity Breakdown of Ultrathin Surface Oxide Films Formed on Ternary Alâ^5%Cuâ^5%Ni Alloys. Journal of Physical Chemistry C, 2010, 114, 17788-17795.	1.5	1
492	Beam damage of HS(CH2)15 COOH Terminated Self Assembled Monolayer (SAM) as Observed by X-ray Photoelectron Spectroscopy. Surface Science Spectra, 2011, 18, 68-81.	0.3	1
493	Effectiveness of high energy ion beam techniques for the characterization of mesoporous low dielectric-constant materials. Nuclear Instruments & Methods in Physics Research B, 2000, 161-163, 476-481.	0.6	0
494	Characterization of ferromagnetic Co-implanted rutile TiO/sub 2/(110). , 0, , .		0
495	Ferromagnetism in Ti-Doped ZnO Nanoclusters above Room Temperature. , 2006, , .		0
496	In-Situ Growth of Passivation Oxide Layer on Fe-Nanoparticle under Electron-Beam Irradiation in a TEM. Microscopy and Microanalysis, 2006, 12, 546-547.	0.2	0
497	Surface and Interface Properties of 10–12 Unit Cells Thick Sputter Deposited Epitaxial CeO ₂ Films. Research Letters in Materials Science, 2008, 2008, 1-5.	0.2	0
498	New Approaches for Characterizing Sensor and Other Modern Complex Materials. ECS Transactions, 2009, 19, 137-148.	0.3	0
499	Combining Raman Microprobe and XPS to Study High-Temperature Oxidation of Metals. ECS Transactions, 2010, 33, 21-29.	0.3	0
500	Enhanced Electron Field Emission from Carbon Nanotube Matrices. Materials Research Society Symposia Proceedings, 2011, 1283, 1.	0.1	0
501	Direct Observation of Li2O2 Nucleation and Growth with In-Situ Liquid ec-(S)TEM. Microscopy and Microanalysis, 2014, 20, 1608-1609.	0.2	0
502	Reply to: "Pitfalls in identifying active catalyst species― Nature Communications, 2020, 11, 4574.	5.8	0
503	Defect-induced anisotropic surface reactivity and ion transfer processes of anatase nanoparticles. Materials Today Chemistry, 2020, 17, 100290.	1.7	0
504	Inhibition of mitochondrial electron transport by atmospheric ultrafine particles: ferrous iron, quinones and ROS production. FASEB Journal, 2008, 22, 264-264.	0.2	0

#	Article	IF	CITATIONS
505	Enabling High-Voltage Lithium Metal Batteries Under Practical Conditions. SSRN Electronic Journal, 0,	0.4	0
506	Preface for the special topic collection honoring Dr. Scott Chambers' 70th birthday and his leadership in the science and technology of oxide thin films. Journal of Vacuum Science and Technology A: Vacuum, Surfaces and Films, 2022, 40, .	0.9	0